Pressure-induced stable structures and physical properties of Sr–Ge system

Shuai Han(韩帅)[1], Shuai Duan(段帅)[1], Yun-Xian Liu(刘云仙)[1,2,†], Chao Wang(王超)[1,2], Xin Chen(陈欣)[1,2], Hai-Rui Sun(孙海瑞)[1,2], and Xiao-Bing Liu(刘晓兵)[1,2,‡]

[1] *Laboratory of High Pressure Physics and Material Science, School of Physics and Physical Engineering, Qufu Normal University, Qufu* 273165, *China*
[2] *Advanced Research Institute of Multidisciplinary Sciences, Qufu Normal University, Qufu* 273165, *China*

(Received 24 March 2022; revised manuscript received 19 April 2022; accepted manuscript online 7 May 2022)

We have systematically investigated the structures of Sr–Ge system under pressures up to 200 GPa and found six stable stoichiometric structures, they being Sr_3Ge, Sr_2Ge, SrGe, $SrGe_2$, $SrGe_3$, and $SrGe_4$. We demonstrate the interesting structure evolution behaviors in Sr–Ge system with the increase of germanium content, Ge atoms arranging into isolated anions in Sr_3Ge, chains in Sr_2Ge, square units in SrGe, trigonal units and hexahedrons in $SrGe_2$, cages in $SrGe_3$, hexagons and Ge_8 rings in $SrGe_4$. The structural diversity produces various manifestations of electronic structures, which is of benefit to electrical transportation. Among them, these novel phases with metallic structures show superconductivity (maximum $T_c \sim 8.94$ K for *Pmmn* Sr_3Ge). Notably, the n-type semiconducting *Pnma* $SrGe_2$ structure exhibits high Seebeck coefficient and excellent electrical conductivity along the *y* direction, leading to a high *ZT* value up to 1.55 at 500 K, which can be potential candidates as high-performance thermoelectrics. Our results will enable the development of fundamental science in condensed matter physics and potential applications in novel electronics or thermoelectric materials.

Keywords: high pressure, first-principle calculation, germanium–strontium compounds, superconductivity, thermoelectric property

PACS: 61.50.Ks, 62.50.–p, 63.20.dk, 71.20.–b **DOI:** 10.1088/1674-1056/ac6db5

1. Introduction

The electronic configuration is an essential quality that determines the material function, while the valence election distributions are influenced by the chemical composition and atomic organization. Compounds formed by the group IV elements with electropositive partners of the alkaline-, alkaline earth-, and rare earth metals exhibit a rich variety of binary systems with semiconductors or metals. In these compounds, tetrel atoms can form different motifs due to rather atypical interactions. Such a rich structural diversity naturally brings interesting physical phenomena and properties, which can be used in solar-cells, thermoelectricity, and optoelectronics.[1,2] For example, an excellent ZT value = 1.1 was achieved in the n-type Mg_2(Si, Sn) system under ambient condition, and they can be seen as promising thermoelectric materials.[3] Both $BaGe_2$ and $SrGe_2$ show high optical absorption coefficients (7.5×10^4 cm^{-1} and 7.8×10^4 cm^{-1} at $\hbar\omega = 1.5$ eV), indicating that they are ideal solar cell candidates.[4]

Pressure has become a useful tool to expand the variety of materials, and modify accessible structure patterns with excellent properties. In recent years, novel stoichiometries with superconductivity were studied in compounds constituted by metals and group IV elements associated with the well-known effect of pressure. Some lanthanide metal germanides with new compositions ($LaGe_3$, $LaGe_5$, $ScGe_2$, YGe_2, YGe_3, $LuGe_2$, $LuGe_3$) were synthesized under high-pressure and high-temperature conditions (HPHT). They all exhibit superconductivity with critical temperature $T_c = 1.3$ K–7.4 K.[5–11] For alkali and alkaline earth metal germanides, they also show novel compositions and properties. For exapmle, a new $BaGe_3$ stoichiometric structure was reported by Castillo *et al.*, with a $T_c = 6.5$ K.[12] Mg–Ge was studied under pressure, in which novel *Cmcm* Mg_2Ge and *P*4/*mmm* MgGe structures are superconductors with T_c of 10.3 K and 9.07 K at 5 GPa.[13] Moreover, in these compounds (alkaline metal, alkaline earth metal and rare earth metal germanides), Ge atoms form different motifs, such as Ge_2 dumbbells, regular triangular Ge_3 cluster units, Ge_4 tetrahedron, Ge_5 square-pyramidal units, edge-sharing Ge_6 rings, Ge_6 octahedrons, Ge–Ge zigzag chains, and Ge cages. These structural polymorphism features completely lead to different bonding arrangements, and could bring various properties.

Owing to a large electronegativity between Sr and Ge atoms, Sr–Ge system can also have structural diversity and rich properties. As is well known, some compositions (such as Sr_2Ge, $SrGe_{2-\delta}$, $SrGe_2$, $SrGe_3$, $SrGe_{6-\delta}$) of Sr–Ge have been studied and synthesized under pressure and show excellent properties.[4,14–18] For instance, *I*4/*mmm* $SrGe_3$ phase was synthesized at 13 GPa and 1100 °C.[14] It showed superconductivity with $T_c = 6.0$ K. $SrGe_{2-\delta}$ was obtained at 2 GPa and 900 °C, which is a superconductor with T_c about

†Corresponding author. E-mail: yunxianliu1988@163.com
‡Corresponding author. E-mail: xiaobing.phy@qfnu.edu.cn

© 2023 Chinese Physical Society and IOP Publishing Ltd

7.3 K.[15] Furthermore, *Pnma* $SrGe_2$, a semiconductor with good optical property, was synthesized by the Ar arc-melting technique.[4] However, some problems remain to be further solved: (i) whether the new Sr–Ge compounds are stable at moderate conditions; (ii) the ground-state structures and properties of Sr–Ge system under high pressure; and (iii) the unit of germanium in the Sr–Ge compounds.

In this work, the Sr–Ge binary system under high-pressure is systematically studied by using the evolutionary algorithm Universal Structure Predictor: Evolutionary Xtallography (USPEX), which has been successfully used in other systems.[19–23] Six stoichimetric structures (Sr_3Ge, Sr_2Ge, SrGe, $SrGe_2$, $SrGe_3$, and $SrGe_4$) are predicted. In these compounds, Ge atoms present diverse motifs forming covalent boding. Metallic structures exhibit superconductivity with T_c of 0.23 K–8.94 K. Semiconductor *Pnma* Sr_2Ge shows a high optical absorption coefficient ($\alpha(\omega) = 1.05 \times 10^5$ cm^{-1} at 1.5 eV). The p-type Sr_2Ge and the n-type $SrGe_2$ exhibit maximal ZT values of about 0.82 and 1.55 along the y direction at 500 K, respectively.

2. Computational details

In the present work, we used the evolutionary method USPEX[24–26] to search for the thermodynamically stable candidates of Sr–Ge system under 0 GPa–200 GPa. Structural optimization and calculation of electronic properties were calculated by the Vienna *ab initio* simulation package (VASP)[27] based on the density functional theory (DFT) framework. The generalized gradient approximation of the Perdew–Burke–Ernzerhof (GGA-PBE)[28] was used to ascertain the exchange correlation functional. And projector-augmented wave (PAW)[29] with $4s^24p^2$ and $4s^24p^65s^2$ electrons was used as valence electrons for Ge and Sr atoms, respectively. A cutoff energy of 500 eV and a k-point grid spacing of $2\pi \times 0.03$ Å^{-1} were used to ensure a good convergence of enthalpy. Phonon calculations were conducted by exercising a supercell technique[30] through using the finite displacement method as accomplished in the PHONOPY code.[31] The integrated crystal orbital Hamilton populations (−ICOHPs) were calculated by LOBSTER package.[32] The electron localization function (ELF)[33] and Bader charge analysis[34–36] were used to analyze the chemical bonds and the electronic charge transfer. Molecular dynamics (MD) simulations were performed in the fixed particle number, volume, and temperature (NVT) ensemble by using the Nose–Hoover thermostat, lasting 9 ps in time steps of 1.5 fs.[37] Quantum ESPRESSO software was used to calculate the electron–phonon coupling (EPC) parameters and phonon dispersion curves.[38] The kinetic energy cutoff was chosen to be 90 Ry. The T_c was estimated from Allen–Dynes-modified McMillan[39] formula

$$T_c = \frac{\omega_{\log}}{1.2} \exp\left[-\frac{1.04(1+\lambda)}{\lambda - \mu^*(1+0.62\lambda)}\right].$$

The absorption coefficient $\alpha(\omega)$ was obtained directly from the calculated complex dielectric function $\varepsilon(\omega) = \varepsilon_1(\omega) + i\varepsilon_2(\omega)$ (where ε_1 is the real part and ε_2 is the imaginary part of ε).[40] Based on a well-converged electronic structure within the dense Monkhorst–Pack k-point spacing of 0.05 Å^{-1}, the transport properties were calculated by BoltzTraP program.[41]

3. Results and discussion

3.1. Phase stability of Sr–Ge compounds under pressure

To find the stable stichiometric structures, we extensively search for each member of Sr_xGe_y (x = 1–3, y = 1; x = 1, y = 2–4) with 1–4 formula units at 0 K, and 0, 50, 100, 150, and 200 GPa. Then the formation enthalpy (ΔH_f) of Sr–Ge system is provided at corresponding pressure. The ΔH_f is calculated according to the following equation:

$$\Delta H_f(Sr_xGe_y) = [H(Sr_xGe_y) - xH(Sr) - yH(Ge)]/(x+y).$$

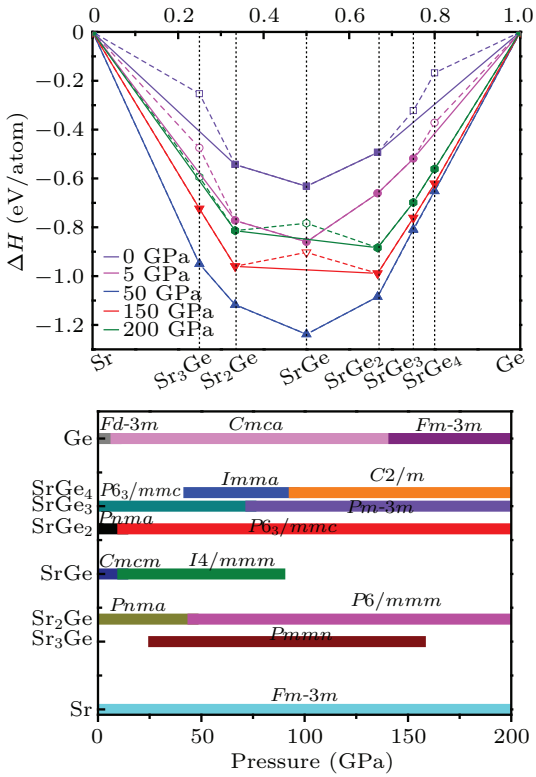


Fig. 1. (a) Relative enthalpies of formation per atom with respect to elemental Ge and Sr for predicted Sr–Ge system at 0, 5, 50, 150, and 200 GPa, with stable compounds represented by solid symbols and connected by solid line (convex hull). (b) Pressure–composition phase diagram of stable Sr–Ge system. *Fm*-3*m* Sr and *Fd*-3*m*, *Cmca*, *Fm*-3*m* Ge are adopted as reference structures.

Because of the formation enthalpies, a convex hull can be created as shown in Fig. 1(a). In general, the thermodynamically stable phases are located on the convex hull, which are

anticipated to be synthesized experimentally. Whereas the unstable or metastable phases are above the convex hull (dotted line), and will decompose into the pure elements and/or compounds located on the hull. At 0 GPa, only Sr_2Ge, SrGe, and $SrGe_2$ are located on the convex hull, which are stable against decomposition. And the already known *Pnma* Sr_2Ge, *Cmcm* SrGe, and *Pnma* $SrGe_2$ are reproduced, which manifests the accuracy of our results. As pressure increases up to 5 GPa, besides the above three stoichiometric structures that remain on the hull, $SrGe_3$ emerges on the convex hull. At 50 GPa, the whole compositions stay on the hull, indicating that they are thermodynamically stable. At 100 GPa and 150 GPa, except that SrGe decomposes into Sr_2Ge and $SrGe_2$, all the other compositions fall on the convex hull. At 200 GPa, there are four compositions (Sr_2Ge, $SrGe_2$, $SrGe_3$, and $SrGe_4$) sitting on the hull. The pressure–composition phase diagram of Sr–Ge system is given in Fig. 1(b).

3.2. Structures and stabilities of Sr–Ge compounds

Besides the known candidate structures (Fig. S1) which are consistent with our predicted results,[4,14,42,43] some new structures were found as shown in Fig. 2. We see that in Sr_3Ge and Sr_2Ge (space group *Pnma*), germanium atoms exist in isolated atomic form, while in other phases Ge atoms present distinct units. For Sr_3Ge, an orthorhombic *Pmmn* (Fig. 2(a)) is predicted, which is stable in a pressure range of 27 GPa–156 GPa. The "isolated" Ge atoms occupy the crystallographic 2*b* sites, while Sr atoms hold 2*a* and 4*f* sites. Figure 2(b) gives the new high-pressure phase of *P*6/*mmm* Sr_2Ge, it remains stable in 46 GPa–200 GPa, in which the Ge atoms form Ge–Ge.Ge linear chains with the shortest Ge–Ge distance of 2.8374 Å. For SrGe stoichiometeric structure, a new phase with *I*4/*mmm* symmetry (Fig. 2(c)) is predicted, where Ge atoms exist in the Ge_4 square units. And it keeps stable from 12 GPa to 88 GPa. Turning to $SrGe_2$, a high phase $P6_3/mmc$ (Fig. 2(d)) is found to be stable in a pressure range from 12 GPa to 200 GPa. It is composed of Sr atoms, Ge_3 trigonal units and the Ge_5 hexahedrons, with three types of Ge–Ge distances, namely 2.330, 2.448, 2.454 Å, respectively. The $P6_3/mmc$ and *Pm*-3*m* phases of $SrGe_3$ are also given in Figs. 2(e) and 2(f), and they are stable in a pressure range of 3 GPa–74 GPa and 74 GPa–200 GPa, respectively. For the former, it contains Ge_3 equilateral triangles with a side length of 2.596 Å, and each layer of Ge triangles is twisted by 60°, which is similar to the scenarios of $BaGe_3$ and $EuGe_3$.[44,45] For the latter, each Ge_{12} cage contains an Sr atom, and the shortest distance between Ge and Ge is 2.630 Å. Turning to $SrGe_4$, the predicted orthorhombic *Imma* (Fig. 2(g)) consists of Ge_8 rings, Ge atoms and Sr atoms and keeps stable at pressures in a range of 45 GPa–95 GPa. Then it transforms into a monoclinic structure with *C*2/*m* symmetry (Fig. 2(h)), in which there are Ge_3 triangles, Ge_6 hexagons, Ge and Sr atoms. As seen in the new predicted Sr–Ge compounds, the Ge atoms' arrangement reveals multiple structure evolution behavior with the increase of germanium content, from isolated anions in Sr_3Ge, chains in Sr_2Ge, square units in SrGe, trigonal units and hexahedrons in $SrGe_2$, cages in $SrGe_3$, and hexagons and Ge_8 rings in $SrGe_4$. These distinct structural features can result in exotic properties. The detailed structural parameters can be obtained in Table S1.

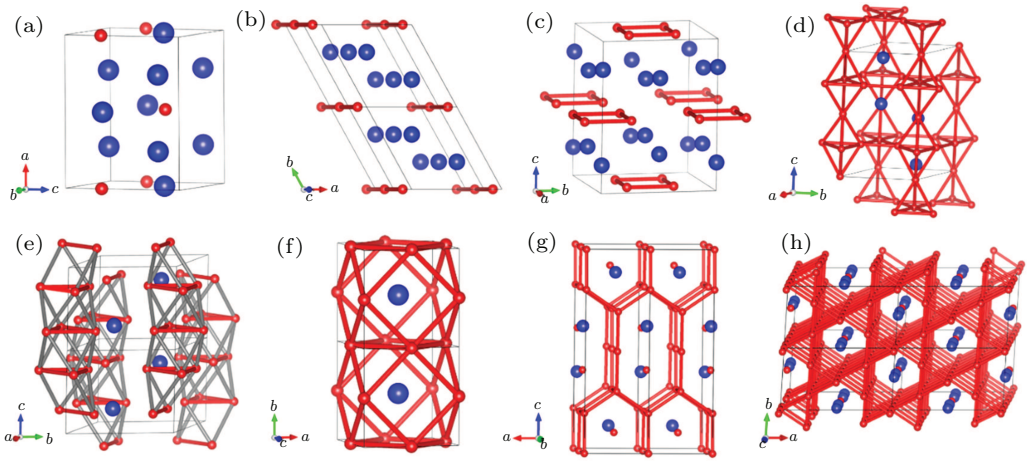


Fig. 2. Crystal structures of Sr–Ge compounds. (a) *Pmmn* Sr_3Ge, (b) *P*6/*mmm* Sr_2Ge, (c) *I*4/*mmm* SrGe, (d) $P6_3/mmc$ $SrGe_2$, (e) $P6_3/mmc$ $SrGe_3$, (f) *Pm*-3*m*$SrGe_3$, (g) *Imma* $SrGe_4$, and (h) *C*2/*m*$SrGe_4$ with large blue and small red balls representing Sr and Ge atoms, respectively.

In order to determine whether the structure satisfies the dynamic stability condition, the phonon spectra and partial phonon density of states (PHDOS) of these structures are calculated. As shown in Fig. S2, no imaginary phonon frequency exists in the whole Brillouin zone, indicating that the above structures are dynamic stable under stable pressure. In addition, on the basis of PHDOS analysis, the motions of Ge and Sr cover almost all frequency regions, which may be caused by the approximate atomic mass of them.

Moreover, the elastic constants C_{ij} are essential for in-

vestigating the mechanical properties. The calculated elastic constants C_{ij} of these Sr–Ge binary structures are listed in Table S3. These values satisfy the Born–Huang criterion,[46,47] indicating that they are all mechanically stable under pressure.

3.3. Electronic properties and chemical bonds of Sr–Ge compounds

In order to understand the electronic properties of Sr–Ge compounds, we calculate the electronic band structures and projected density of states (PDOS). From Fig. S3, we see that *Pnma* Sr_2Ge and *Pnma* $SrGe_2$ are semiconductors, in which the band gaps are located almost in the center of Brillouin zone. While the other structures show metallic behaviors with their valence bands and conduction bands overlap. In the following, we mainly focus on the metallic phases of *P6/mmm* Sr_2Ge (Ge-rich compound), *P6*$_3$*/mmc* $SrGe_3$, and *Pm-3m* $SrGe_3$ (Sr-rich compounds) because of their wide stable pressure ranges and different Ge motifs, as well as two semiconductors of *Pnma* Sr_2Ge and *Pnma* $SrGe_2$. The electron properties of the other predicted Sr–Ge compounds are given in the supplement materials.

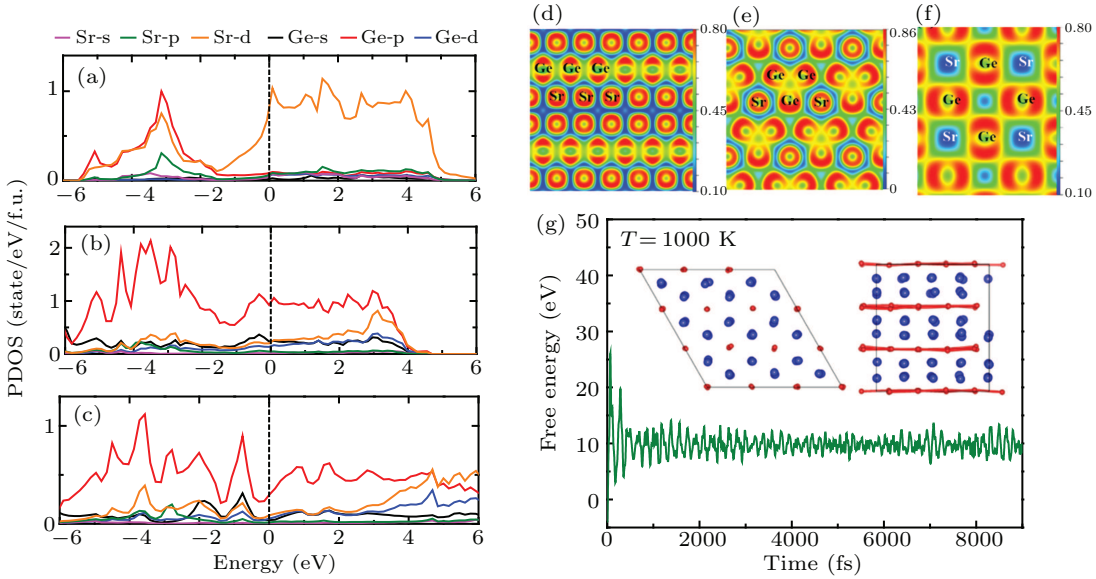


Fig. 3. Calculated projected density of states (PDOS) of (a) *P6/mmm* Sr_2Ge, (b) *P6*$_3$*/mmc* $SrGe_3$, and (c) *Pm-3m*$SrGe_3$. The electron localization function (ELF) plotted on (d) (–1 –1 0) plane of *P6/mmm* Sr_2Ge, (e) (0 0 –1) plane of *P6*$_3$*/mmc* $SrGe_3$, and (f) (0 0 –1) plane of *Pm-3m* $SrGe_3$. (g) Free energy as MD time at temperature of 1000 K and structure snapshots taken after equilibration of *P6/mmm* Sr_2Ge.

The calculated projected densities of states are shown in Fig. 3. For *P6/mmm* Sr_2Ge and *P6*$_3$*/mmc* $SrGe_3$, *Pm-3m* $SrGe_3$, the states around the Fermi level are mainly composed of Sr-d and Ge-p orbitals with almost no Sr-s component, demonstrating that the 5s electrons of Sr are nearly transferred to the Ge unites. Then, the electron localization function (ELF) calculations are performed to study the bond nature. Generally, larger ELF values (> 0.5) usually correspond to inner shell, lone pair electrons and covalent bonds, whereas the ionic and metallic bonds correspond to small ELF values (< 0.5). The ELF calculations show that Ge–Ge bonds are covalent in *P6/mmm* Sr_2Ge and *P6*$_3$*/mmc* $SrGe_3$, *Pm-3m* $SrGe_3$ (Figs. 3(d)–3(f)), while the Sr–Ge bonding is weakly ionic. The calculated projected crystal orbital Hamilton population (pCOHP) are shown in Fig. S6. We see that most of the states below the Fermi level correspond to Ge–Ge bonding, which sustains the existence of Ge–Ge covalent bonds within the Ge units. Bader charge analysis shows that charges transfer from Sr atoms to the Ge atoms as given in Table S2, supporting the above PDOS's analyzing. In addition, first-principles molecular dynamics (MD) simulations are performed to verify their thermal stability at 600 K and 1000 K by using the NVT ensemble and Nose–Hoover thermostat. The MD time step is 1.5 fs, and we monitor the time evolution of free energy during the MD simulations as shown in Figs. 3(g) and S7. The free energy values reach equilibrium speedily and fluctuate near the equilibrium value with no structural reconstructions, which indicates that the *P6/mmm* Sr_2Ge and *P6*$_3$*/mmc* $SrGe_3$, *Pm-3m* $SrGe_3$ remain stable at these temperatures.

3.4. Superconductivity of Sr–Ge compounds

To explore the possibility of phonon-mediated superconductivity in the predicted phases of *P6/mmm* Sr_2Ge, *P6*$_3$*/mmc* $SrGe_3$, and *Pm-3m* $SrGe_3$, we calculate the electron–phonon coupling (EPC) parameter (λ), the logarithmic mean phonon frequency ($\omega_{\log}$), the electron density of states at the Fermi level ($N(E_f)$), and the superconducting critical temperature (T_c). Figure 4(a) gives the calculated values of λ, $\omega_{\log}$, $N(E_f)$, and T_c as a function of pressure for *P6/mmm* Sr_2Ge, to investigate the effect of pressure on superconductivity. The result shows that the calculated T_c value increases and then decreases with pressure increasing. As seen, the tendency of λ is similar to T_c upon compression. Therefore, we think that the variation

of the T_c values with pressure may mainly be due to the λ. As is well known, the "softness" of phonon dispersion can result in strengthening EPC (λ). Then the phonon dispersion curves at different pressures are calculated, and the results are given in Figs. 4b–4(e). It is found that the λ is mainly form the contribution of low-frequency phonon modes, which is dominated by Sr atoms. In addition, we see that "softness" behavior occurs in low-frequency vibrations along $K \rightarrow H$ direction from 50 GPa to 150 GPa, and then vanishes at 200 GPa, which leads to the increase/decrease in λ with pressure increasing.

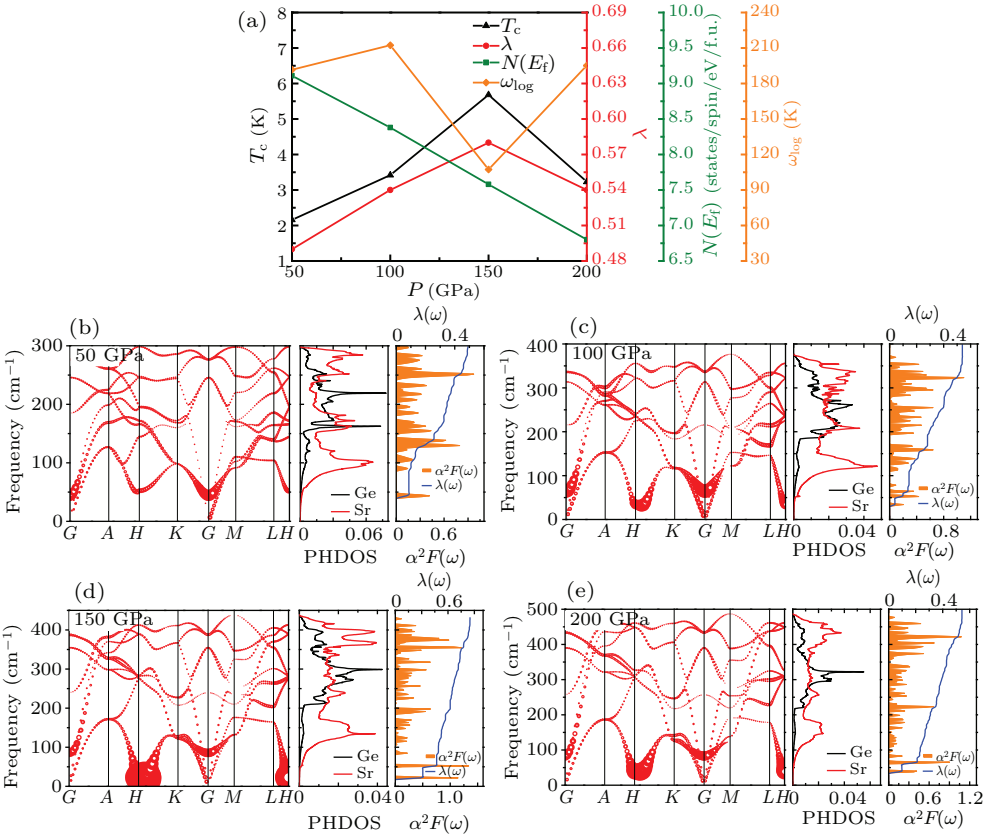


Fig. 4. (a) Calculated values of λ, ω_{log}, $N(E_f)$, and T_c as a function of pressure for *P*6/*mmm* Sr_2Ge. *P*6/*mmm* Sr_2Ge phonon dispersion curves at (b) 50 GPa, (c) 100 GPa, (d) 150 GPa, and (e) 200 GPa. Red circle on phonon dispersion curve represents the discrete electron–phonon coupling, electro–acoustic coupling parameters, and the size of red circle is proportional to the strength of electron–phonon coupling electro–acoustic coupling.

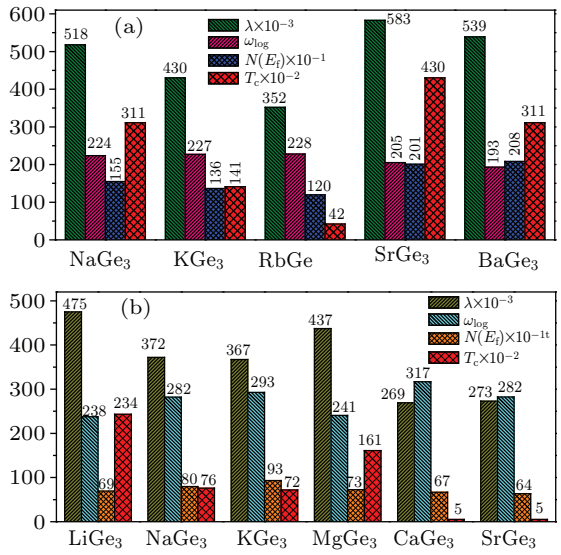


Fig. 5. Electron–phonon coupling parameters (λ), logarithmic average phonon frequency (ω_{log}), electronic density of states at the Fermi level ($N(E_f)$) (states/spin/Ry/unit cell), and superconducting critical temperatures (T_c) for (a) $P6_3/mmc$ XGe_3 (X = Na, K, Rb, Sr, Ba) at 50 GPa and (b) *Pm*-3*m* MGe_3 (M = Li, Na, K, Mg, Ca, Sr) at 100 GPa.

Based on the fact that $P6_3/mmc$ $SrGe_3$ appears in other systems ($BaGe_3$ and $EuGe_3$), as well as the cages forming in *Pm*-3*m* $SrGe_3$, we then construct some hypothetical models of $P6_3/mmc$ XGe_3 and *Pm*-3*m* XGe_3, where X denotes alkali metal elements and alkaline earth elements. The calculated phonon dispersion curves show that $P6_3/mmc$ XGe_3 (X = Na, K, Rb, Ba) and *Pm*-3*m* MGe_3 (M = Li, Na, K, Mg, Ca) remain stable at different pressures (Fig. S8). Moreover, they all exhibit metallic feature (Fig. S9). To investigate their superconductivities, and the values of λ, ω_{log}, $N(E_f)$, and T_c at different pressures are shown in Fig. 5. It can be seen that $P6_3/mmc$ $SrGe_3$ and *Pm*-3*m*$NaGe_3$ have highest values of T_c of 4.3 K and 2.3 K in the $P6_3/mmc$ XGe_3 hypothetical model and *Pm*-3*m* MGe_3 hypothetical model, respectively. Moreover, we find that for both $P6_3/mmc$ XGe_3 phase and *Pm*-3*m* MGe_3 phase, the T_c values are mainly influenced by the value of λ. In other words, the bigger the value of λ, the higher the temperature T_c is. For other predicted phases of Sr–Ge system, the λ, ω_{log}, $N(E_f)$, and T_c values are listed in Table S3.

3.5. Potential optical and thermoelectric application of *Pnma* Sr_2Ge and *Pnma* $SrGe_2$

On the basis of the above discussion, we calculate the optical and thermoelectric properties of *Pnma* Sr_2Ge and *Pnma* $SrGe_2$. The fundamental band gap is $E_g = 0.78$ eV for Sr_2Ge (Fig. S10) and $E_g = 0.89$ eV for $SrGe_2$.[4] Extensive researches have been carried out in the past decades on metal germanides to investigate their optical properties,[4,48] such as $SrGe_2$, $BaGe_2$, Ca_2Ge. We calculate the absorption coefficient of Sr_2Ge with the help of HSE06 functional. It does not show any sizable anisotropy like some other metal germanides. As shown in Fig. S11, the average polarization-independent absorption of *Pnma* Sr_2Ge is $\alpha(\omega) = 1.05 \times 10^5$ cm^{-1} at 1.5 eV. The large absorption coefficient reveals its better optical properties, indicating that the *Pnma* Sr_2Ge has a potential application prospect in solar-cells.

Here, we illustrate the calculated band structures and electrical transport coefficients for the *Pnma* Sr_2Ge and *Pnma* $SrGe_2$ in Figs. 6 and S12–S14. Interestingly, the $SrGe_2$ exhibits a multi-valley conduction band structure near Fermi level, realizes high-valley degeneracy with small energy difference and possess more states for electrons to occupy and contribute to transport, which is of great help in improving thermoelectric performance. Furthermore, we can notice from the calculated partial DOS in Fig. 6 that the coupling between d state of Sr atom and p state of Ge atom in $SrGe_2$ is stronger than in Sr_2Ge. Therefore, the $SrGe_2$ has a much steeper DOS for the bottom of the conduction band (CB) than pristine $SrGe_2$, indicating a higher room-temperature Seebeck coefficient in $SrGe_2$ system.

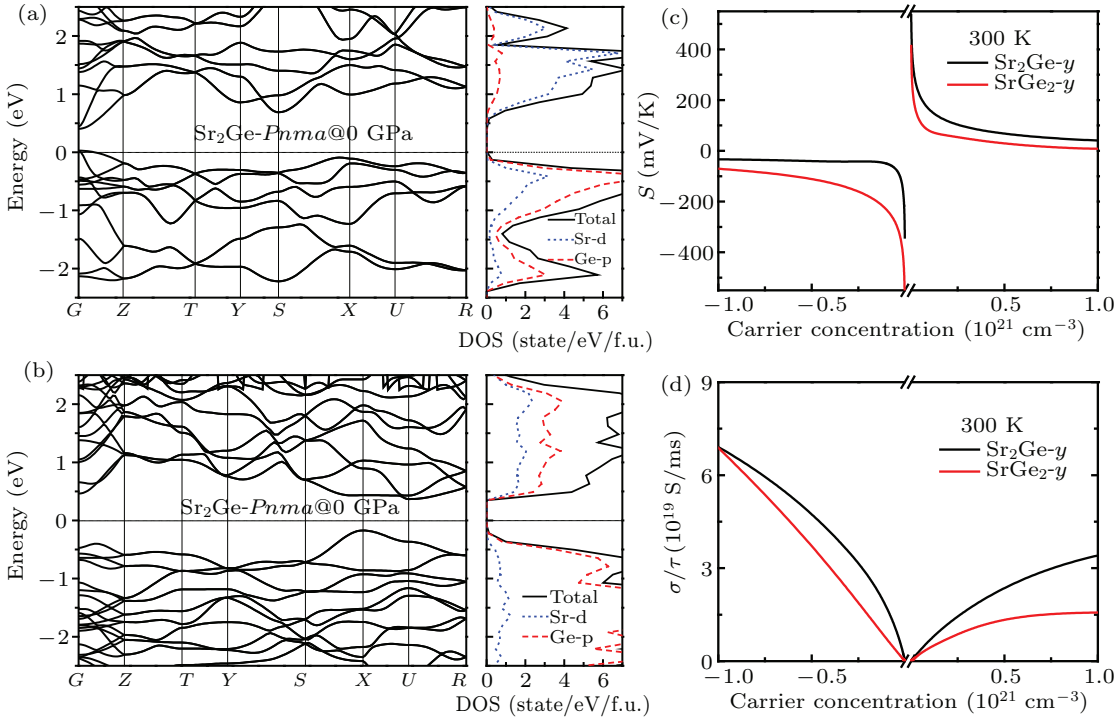


Fig. 6. PBE functional calculated band structures and density of states for (a) *Pnma* Sr_2Ge and (b) *Pnma* $SrGe_2$. (c) and (d) PBE functional calculated Seebeck coefficient and electrical conductivity varying with carrier concentration in the *y* direction at 300 K for *Pnma* Sr_2Ge and *Pnma* $SrGe_2$, respectively.

From the electronic structures discussed above, it can be seen from Fig. 6(c) that $SrGe_2$ exhibits the highest Seebeck coefficient along the *y* direction within electron doping, derived from the flat conduction band dispersions and sharp DOS near CBM as shown in Fig. 6(b). A high Seebeck coefficient can reach up to -230 μV/K with the electron doping of 1.03×10^{20} cm^{-3} at 300 K, roughly 4.65 times larger than the counterpart that Sr_2Ge has. For *x* direction and *z* direction, the Seebeck coefficient of n-type $SrGe_2$ is also much larger than that of Sr_2Ge, as shown in Figs. S12(a) and S12(b). Moreover, we note that the $SrGe_2$ has great electrical conductivity, which is mainly attributed to their favorable electronic band structures, like multi-valley conduction band structures. Combined with the Seebeck coefficients discussed above, our current results indicate that the n-type $SrGe_2$ can have better thermoelectric performance than the Sr_2Ge, particularly along the *y* direction.

Based on the electrical transport coefficients discussed above, the thermoelectric performance can be quantitatively estimated from

$$ZT = \frac{S^2(\sigma/\tau)T}{L_0(\sigma/\tau)T + \kappa_L/\tau},$$

where L_0 ($= 2.45 \times 10^{-8}$ WΩ/K^2) is the Lorenz number. The lattice thermal conductivity with respect to scattering time $\kappa_L/\tau = 10^{14}$ W·m^{-1}·K^{-1}·s^{-1} is used. For the comprehensive analysis, the calculated *ZT* values for *Pnma* Sr_2Ge and *Pnma*

$SrGe_2$ are shown in Table 1. We note that the n-type $SrGe_2$ has the uppermost ZT value of 0.76 along the y direction at 300 K, distinctly larger than the highest value of 0.17 in n-type Sr_2Ge. When temperature increases to 500 K, a higher ZT value (1.55) can be obtained in n-type $SrGe_2$, roughly 3.37 times larger than the counterpart of Sr_2Ge.

Table 1. Optimized ZT values of *Pnma* Sr_2Ge and *Pnma* $SrGe_2$ at 300 K and 500 K along x, y, and z directions.

System	Direction	Carrier	n (cm^{-3})-300 K	ZT-300 K	n (cm^{-3})-500 K	ZT-500 K
Sr_2Ge	x	n-type	3.98×10^{20}	0.08	2.96×10^{19}	0.23
		p-type	4.06×10^{19}	0.36	6.21×10^{19}	0.69
	y	n-type	8.04×10^{18}	0.17	1.19×10^{19}	0.46
		p-type	5.15×10^{19}	0.39	7.71×10^{19}	0.82
	z	n-type	3.36×10^{20}	0.12	2.69×10^{20}	0.29
		p-type	9.91×10^{20}	0.12	9.72×10^{20}	0.41
$SrGe_2$	x	n-type	1.98×10^{20}	0.25	2.09×10^{20}	0.60
		p-type	1.33×10^{19}	0.25	1.90×10^{19}	0.60
	y	n-type	1.03×10^{20}	0.76	8.87×10^{19}	1.55
		p-type	2.69×10^{19}	0.09	3.78×10^{19}	0.25
	z	n-type	5.69×10^{19}	0.56	7.40×10^{19}	1.25
		p-type	2.17×10^{19}	0.07	3.48×10^{19}	0.20

4. Conclusions

In summary, we have reported the phase diagram, crystal structure and physical properties in Sr–Ge system at pressures ranging from 0 GPa to 200 GPa. We predict six stable compounds (Sr_3Ge, Sr_2Ge, SrGe, $SrGe_2$, $SrGe_3$, $SrGe_4$) by first-principles calculations. Our results reveal that multiple Ge units in diverse structures (Ge_2, Ge_3, Ge_4, Ge–Ge...Ge chains, Ge cage, *etc*.) can be formed by covalent bonds under high pressure conditions. Among them, most of Sr–Ge phases exhibit superconducting behaviors ($T_c = 0.23$ K–8.94 K). A semiconducting structure of *Pnma* Sr_2Ge shows a high optical absorption coefficient $\alpha(\omega) = 1.05\times10^5$ cm^{-1} at 1.5 eV. Most importantly, the p-type Sr_2Ge and the n-type $SrGe_2$ exhibit maximal ZT values of 0.82 and 1.55, respectively, along the y direction at 500 K, implying potential candidates serving as high-performance thermoelectrics.

Acknowledgements

Theoretical calculations were performed in the High Performance Computing Center (HPCC) of Qufu Normal University.

Project supported by the National Natural Science Foundation of China (Grant Nos. 52102335, 11704220, 11804184, 11974208, and 11804185) and the Shandong Provincial Natural Science Foundation, China (Grant Nos. ZR2021MA050, ZR2017BA020, ZR2018PA010, ZR2019MA054, and ZR2017BA012).

References

[1] Hao C M, Li Y, Huang H M and Li Y L 2018 *J. Chem. Phys.* **148** 204706
[2] Shi J, Cui W, Flores-Livas J A, San-Miguel A, Botti S and Marques M A L 2016 *Phys. Chem. Chem. Phys.* **18** 8108
[3] Zaitsev V K, Fedorov M I, Gurieva E A, Eremin I S, Konstantinov P P, Samunin A Y and Vedernikov M V 2006 *Phys. Rev. B* **74** 045207
[4] Kumar M, Umezawa N and Imai M 2015 *J. Alloys Compd.* **630** 126
[5] Fukuoka H, Suekuni K, Onimaru T and Inumaru K 2011 *Inorg. Chem.* **50** 3901
[6] Fukuoka H and Yamanaka S 2003 *Phys. Rev. B* **67** 094501
[7] Meier K, Cardoso-Gil R, Schnelle W, Rosner H, Burkhardt U and Schwarz U 2010 *Z. Anorg. Allg. Chem.* **636** 1466
[8] Matthias B T, Corenzwit E and Zachariasen W H 1958 *Phys. Rev.* **112** 89
[9] Wei M S, Sung H H and Lee W H 2005 *Physica C* **424** 25
[10] Chung Y R, Sung H H and Lee W H 2004 *Phys. Rev. B* **70** 052511
[11] Hübner J M, Bobnar M, Akselrud L, Prots Y, Grin Y and Schwarz U 2018 *Inorg. Chem.* **57** 10295
[12] Castillo R, Baranov A I, Burkhardt U, Cardoso-Gil R, Schnelle W, Bobnar M and Schwarz U 2016 *Inorg. Chem.* **55** 4498
[13] Wang C, Liu Y, Lv P, Sun H and Duan D 2018 *Chem. Eur. J.* **24** 18757
[14] Nishikawa T, Fukuoka H and Inumaru K 2015 *Inorg. Chem.* **54** 7433
[15] Iyo A, Hase I, Kawashima K, Ishida S, Kito H, Takeshita N, Oka K, Fujihisa H, Gotoh Y, Yoshida Y and Eisaki H 2017 *Inorg. Chem.* **56** 8590
[16] Ud Din H, Reshak A H, Murtaza G, Amin B, Ali R, Alahmed Z A, Chysky J, Bila J and Kamarudin H 2015 *Indian J. Phys.* **89** 369
[17] Evers J, Oehlinger G and Weiss A 1979 *Z. Naturforsch B* **34** 524
[18] Hase I, Yanagisawa T, Iyo A, Eisaki H, Yoshida Y and Kawashima K 2018 *J. Phys. Conf. Ser.* **1054** 012004
[19] Liu Y X, Wang C, Han S, Chen X, Sun H R and Liu X B 2021 *Chin. Phys. Lett.* **38** 036201
[20] Wang C, Liu Y X, Chen X, Lv P, Sun H R and Liu X B 2020 *Chin. Phys. Lett.* **37** 026201
[21] Chu B H, Zhao Y, Yan J L and Li D 2018 *Chin. Phys. Lett.* **35** 016401
[22] Sun G L, Huang H M and Li Y L 2016 *Chin. Phys. Lett.* **33** 026104
[23] Lu M, Huang Y, Tian F, Li D, Duan D, Zhou Q and Cui T 2020 *Chin. Phys. B* **29** 053104
[24] Oganov A R and Glass C W 2006 *J. Chem. Phys.* **124** 244704
[25] Oganov A R, Lyakhov A O and Valle M 2011 *Acc. Chem. Res.* **44** 227
[26] Lyakhov A O, Oganov A R, Stokes H T and Zhu Q 2013 *Comput. Phys. Commun.* **184** 1172
[27] Kresse G and Furthmüller J 1996 *Comput. Mater. Sci.* **6** 15
[28] Perdew J P, Burke K and Ernzerhof M 1996 *Phys. Rev. Lett.* **77** 3865
[29] Kresse G and Joubert D 1999 *Phys. Rev. B* **59** 1758
[30] Parlinski K, Li Z Q and Kawazoe Y 1997 *Phys. Rev. Lett.* **78** 4063
[31] Togo A, Oba F and Tanaka I 2008 *Phys. Rev. B* **78** 134106
[32] Dronskowski R and Bloechl P E 1993 *J. Phys. Chem.* **97** 8617
[33] Becke A D and Edgecombe K E 1990 *J. Chem. Phys.* **92** 5397
[34] Bader R F W 1985 *Acc. Chem. Res.* **18** 9
[35] Henkelman G, Arnaldsson A and Jónsson H 2006 *Comput. Mater. Sci.* **36** 354

[36] Tang W, Sanville E and Henkelman G 2009 *J. Phys.: Condens. Matter* **21** 084204
[37] Martyna G J, Klein M L and Tuckerman M 1992 *J. Chem. Phys.* **97** 2635
[38] Giannozzi P, Baroni S, Bonini N, Calandra M, Car R, Cavazzoni C, Ceresoli D, Chiarotti G L, Cococcioni M, Dabo I, Dal Corso A, de Gironcoli S, Fabris S, Fratesi G, Gebauer R, Gerstmann U, Gougoussis C, Kokalj A, Lazzeri M, Martin-Samos L, Marzari N, Mauri F, Mazzarello R, Paolini S, Pasquarello A, Paulatto L, Sbraccia C, Scandolo S, Sclauzero G, Seitsonen A P, Smogunov A, Umari P and Wentzcovitch R M 2009 *J. Phys.: Condens. Matter* **21** 395502
[39] Allen P B and Dynes R C 1975 *Phys. Rev. B* **12** 905
[40] Kumar M, Zhao H and Persson C 2013 *Semicond. Sci. Technol.* **28** 065003
[41] Madsen G K H and Singh D J 2006 *Comput. Phys. Commun.* **175** 67
[42] Betz A, Schäfer H and Weiss A 1967 *Z. Naturforsch B* **22** 103
[43] Ud Din H, Reshak A H, Murtaza G, Amin B, Ali R, Alahmed Z A, Chysky J, Bila J and Kamarudin H 2015 *Indian J. Phys.* **89** 369
[44] Castillo R, Baranov A I, Burkhardt U, Grin Y and Schwarz U 2015 *Z. Anorg. Allg. Chem.* **641** 355
[45] Fukuoka H, Tomomitsu Y and Inumaru K 2011 *Inorg. Chem.* **50** 6372
[46] Zhang Y, Lin S, Zou M, Liu M, Xu M, Shen P, Hao J and Li Y 2021 *Chin. Phys. Lett.* **38** 018101
[47] Wu Z J, Zhao E J, Xiang H P, Hao X F, Liu X J and Meng J 2007 *Phys. Rev. B* **76** 054115
[48] Lyu L, Yang Y, Cen W, Yao B and Ou J 2020 *Mater. Res. Express.* **7** 126304